ISSN 1330-3651 (Print), ISSN 1848-6339 (Online)
UDC/UDK 621.438.057:519.876.5

COMBUSTION OF REFORMED GAS AND LIQUID FUEL IN CRGT COMBUSTOR

Gang Pan, Hongtao Zheng

Original scientific paper
Numerical simulations of four combustion processes in a dual-fuel combustor of chemically recuperated gas turbine (CRGT) were carried out in this work. The fuels in the four combustion processes were liquid fuel, liquid fuel + steam, liquid fuel + reformed gas and reformed gas, respectively. The mathematical models adopted for different fuels combustion consist of realizable $k-\varepsilon$ turbulence model and probability density function (PDF) model. The temperature distribution, species concentrations and NO emission were obtained. The results show that the fuels can burn effectively in the dual-fuel combustor for CRGT. Compared with the liquid fuel combustor, the flame temperature, average temperature of combustor wall and NO emission are reduced by 7,8 %, 4,8 % and 75,3 % respectively when the steam is injected into the combustor. However, they are reduced more when the liquid fuel is replaced by reformed gas, which are 10,3 %, 5,6 % and 97,2 % respectively. A little deterioration of the overall temperature distribution of combustor outlet is obtained for liquid fuel + steam combustor, while a better temperature distribution of combustor outlet is obtained for reformed gas combustor, in comparison with liquid fuel combustor.

Keywords: *dual-fuel combustor, NO emission, numerical simulation, reformed gas, steam injection*

Izgaranje poboljšanog plina i tekućeg goriva u CRGT komori izgaranja

Izvorni znanstveni članak
U ovom su radu provedene numeričke simulacije četiriju procesa izgaranja u komori izgaranja s dvodijelnom sapnicom za gorivo kemijski rekuperirane plinske turbine (CRGT). Goriva u ta četiri procesa izgaranja bila su tekuće gorivo, tekuće gorivo + para, tekuće gorivo + poboljšani (reformirani) plin i reformirani plin. Matematički modeli primijenjeni za izgaranje različitih goriva sastoje se od modela ostvarive $k-\varepsilon$ turbulencije i modela funkcije gustoće vjerovatnoće (PDF). Dobivene su raspodjela temperature, koncentracije vrsta i emisije NO. Rezultati pokazuju da goriva mogu učinkovito sagorijevati u dvodijelnoj komori izgaranja za CRGT. U usporedbi s komorom izgaranja tekućeg goriva, temperatura plamena, srednja temperature stijenke komore izgaranja i emisija NO smanjeni su za 7,8 %, 4,8 % i 75,3 % kad se u komoru uštrcala para. Međutim ti su se iznosi još smanjili kad se tekuće gorivo zamijenilo poboljšanim (reformiranim) plinom i iznosili su 10,3 %, 5,6 % i 97,2 %. Malo pogoršanje ukupne raspodjele temperature ispuha komore izgaranja dobilo se kod komore izgaranja tekućeg goriva + para, dok se bolja raspodjela temperature na ispuhu postigla kod komore izgaranja reformiranog plina u usporedbi s izgaranjem tekućeg goriva.

Ključne riječi: *emisija NO, komora izgaranja s dvodijelnom sapnicom za gorivo, numerička simulacija, poboljšani (reformirani) plin, uštrcavanje pare*

1 Introduction

Thermal efficiency improvement and pollutant emissions control have become issues of global concern due to the world-wide increasing utilization of fossil fuels [1]. In order to improve thermal efficiency and reduce emission of the gas turbine, the CRGT cycle has been presented [2]. Concerning CRGT cycle, firstly, the gas turbine is started with liquid fuel. Secondly, the exhaust heat of flue gas converts the water in the evaporator into steam, which can be injected into the combustor or reformer directly. Thirdly, the steam and liquid fuel in the reformer are heated by flue gas, and an endothermic reaction occurs between them. Then the reformed gas including plenty of steam and hydrogen is obtained, which will be fed into the combustor. Finally, when the CRGT cycle runs stably, the combustor burns the reformed gas only. Obviously, there will be four combustion processes in the CRGT combustor, such as liquid fuel, liquid fuel + steam, liquid fuel + reformed gas and reformed gas. So, in order to ensure the CRGT cycle runs stably, it is important to analyse in detail the effects in the combustion process when using different fuels, as well as in different conditions.

Numerical modelling is an important tool in design and optimization of gas turbine combustor. Advances in computational modelling have resulted in an extensive application of numerical simulations to gas turbine combustors, providing insights and improving the understanding of the combustion process. So far many scholars have employed the method of numerical simulation to analyse the combustion process in combustor with different fuels. These investigations provided detailed descriptions for temperatures, velocities, species concentration fields within various geometries of combustors. Sharma et al. [3] investigated the influences of fuel volatility and spray parameters on combustion characteristics and NOx emission in a combustor. Li et al. [4] carried out numerical investigation on the combustion and cooling performance in an aero-engine annular combustor. Benini et al. [5] has carried out numerical and experimental investigation of the NO emission in a turbojet combustor with the steam injection. The results showed that steam injection is an effective way for controlling the NO emission, which is also showed by Furuhata et al. [6] through experiment. Koyama et al. [7] performed numerical and experimental investigation of a dual fuel combustor, with emphasis on the digester gas concentration and velocity distributions. Gobbato et al. [8] presented a CFD simulation of the air-hydrogen combustion flow field inside a single-can gas turbine combustor. Seibert et al. [9] investigated the effect of using hydrogen or hydrogen-rich reformate as a supplication to JP-8 in a swirling combustor on energy efficiency, operational flexibility and environmental protection. The results showed that the flame stability and fuel efficiency were improved and emissions were reduced at lean conditions with small amounts of hydrogen or reformed JP-8. Ghenai [10] studied the effects of fuels with different composition and heating value on the combustion and emission performance of a gas turbine can combustor. Wang et al. [11] and Tanaka et

al. [12] both performed a direct numerical simulation of a hydrogen/air premixed flame in a micro combustor. They both showed the flow characteristics and flame structure properties in the flame. Furthermore, the latter has investigated the influence of swirl number on these characteristics. Arghode et al. [13] investigated the velocity distribution in a CDC combustor numerically. Kumar et al. [14] conducted a numerical analysis of an axisymmetric trapped vortex combustor, and the effect of secondary air jet momentum on the flow structure in the combustor was investigated. Cameretti et al. [15] investigated the performance of a lean-premixed combustor with bio-fuels, and investigated the effect of methods for supplying fuel on the temperature, fuel concentration and NO mass fraction distribution.

In this paper, numerical simulations of four combustion processes inside a CRGT combustor have been carried out, and the flame temperature, species concentrations and NO emission are obtained. This work can provide theoretical support for the optimal design of CRGT combustor and the rational use of different fuels in the combustor.

2 Physical and mathematical modelling

2.1 Geometry and mesh

As shown in Fig. 1, the combustor with a dual-fuel nozzle for the CRGT was employed in this study. The dual-fuel nozzle can spray both liquid and gas fuels into the combustor. The lengths of the combustor in the *X*, *Y* and *Z* direction are 743, 245 and 391 mm respectively.

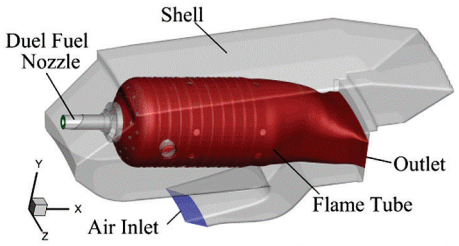

Figure 1 The dual-fuel combustor

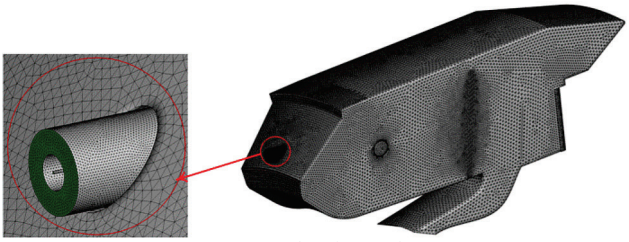

Figure 2 Meshes for combustor

Unstructured tetrahedral meshes were employed for this numerical simulation. Fig. 2 shows the tetrahedral meshes for the dual-fuel combustor. In order to obtain the maximum resolution of dual-fuel nozzle and film cooling holes, the grid is denser near these components of the geometry. The total grid number is 3 500 000.

2.2 Mathematical modelling

2.2.1 Governing equations

In this work, the reacting flow is assumed to be steady-state and the combustion is assumed to be adiabatic. The effect of gravity and the radiation heat transfer are also neglected. The equations of mass, momentum and energy conservation can be expressed as follows [16]:

Continuity equation

$$\nabla \cdot (\rho \vec{v}) = S_m. \tag{1}$$

Momentum conservation equation

$$\nabla \cdot (\rho \vec{v} \vec{v}) = -\nabla p + \nabla \boldsymbol{\tau} + \vec{F}. \tag{2}$$

Energy conservation equation

$$\nabla \cdot (\rho \vec{v} E) = \nabla \cdot \left(\kappa_{\text{eff}} \nabla T - \sum_{i=1}^{N_S} h_i \vec{J}_i + \boldsymbol{\tau} \vec{v} - p \vec{v} \right) + S_h. \tag{3}$$

State equation:

$$p = \sum_{i=1}^{N_S} \rho m_i \frac{RT}{M_i}. \tag{4}$$

where, ρ represent density and p static pressure respectively, $\vec{v}$ is the velocity, S_m is mass added to the continuous phase from the dispersed second phase, $\boldsymbol{\tau}$ is the stress tensor, $\vec{F}$ is momentum source, E is the total specific energy, κ_{eff} is the effective conductivity, h_i is the sensible enthalpy of species i, $\vec{J}_i$ is the diffusion flux of species i, S_h is energy source, m_i is the mass fraction of species i, R is the universal constant, M_i is the molecular weight, N_S is the total number of species.

In this work, the CFD software FLUENT has been applied to study the combustion flow field of the dual-fuel combustor. In order to discretize the governing equations, the finite volume method and upwind scheme were adopted. The SIMPLE (semi implicit method for pressure linked equations) algorithm was employed to couple the velocity field and pressure.

2.2.2 Turbulence model

The realizable $k - \varepsilon$ model [17] was selected to describe the turbulence flow in the combustor. In comparison with the standard $k - \varepsilon$ model, the realizable $k - \varepsilon$ model contains an alternative formulation for the turbulent viscosity and the transport equation for the dissipation rate is modified. The transport equations are as follows:

$$\nabla \cdot (\rho \vec{v} k) = \nabla \cdot \left[\left(\mu + \frac{\mu_t}{\sigma_k} \right) \nabla k \right] + G_k + G_b - \rho \varepsilon - Y_k + S_k, \tag{5}$$

$$\nabla \cdot (\rho \vec{v} \varepsilon) = \nabla \cdot \left[\left(\mu + \frac{\mu_t}{\sigma_\varepsilon} \right) \nabla \varepsilon \right] + \rho C_1 S \varepsilon - \rho C_2 \frac{\varepsilon^2}{k + \sqrt{\nu \varepsilon}} + \tag{6}$$

$$+ C_{1\varepsilon} \frac{\varepsilon}{k} C_{3\varepsilon} G_b + S_\varepsilon,$$

where k and ε are the turbulence kinetic energy and turbulence dissipation rate, respectively, μ and μ_t are dynamic and eddy viscosity, respectively, G_k and G_b represent the generation of turbulence kinetic energy due to the mean velocity gradients and buoyancy, respectively, Y_k represents the contribution of the fluctuating dilatation in compressible turbulence to the overall dissipation rate, S_k and S_ε are user-defined source terms, $C_{1\varepsilon}$=1,44, C_2=1,9, σ_k=1,0, σ_ε=1,2.

2.2.3 Combustion model

The probability density function (PDF) model [10] was adopted. The transport equations for the mixture fraction and its variance are as follows:

$$\nabla\cdot(\rho\vec{v}\overline{f}) = \nabla\cdot\left(\frac{\mu_t}{\sigma_t}\nabla\overline{f}\right) + S_m + S_{\text{user}}, \tag{7}$$

$$\nabla\cdot(\rho\vec{v}\overline{f'^2}) = \nabla\cdot\left(\frac{\mu_t}{\sigma_t}\nabla\overline{f'^2}\right) + C_g\mu_t(\nabla\overline{f})^2 - \\ - C_d\rho\frac{\varepsilon}{k}\overline{f'^2} + S_{\text{user}}, \tag{8}$$

where $\overline{f}$ and $\overline{f'^2}$ are mixture fraction and mixture fraction variance respectively, S_{user} is user-defined source term. The constant values of, σ_t, C_g and C_d are 0,85; 2,86 and 2,0, respectively.

2.2.4 NOx formation

Due to the low NO concentration, the effect of NOx formation process on the flow field is neglected. So the prediction of NO is post processed from the simulation. In this paper, the thermal and prompt mechanisms of NO formation were adopted [18]. For thermal and prompt NOx mechanisms, only the NO species transport equation is needed:

$$\nabla\cdot(\rho\vec{v}Y_{\text{NO}}) = \nabla\cdot(\rho D\nabla Y_{\text{NO}}) + S_{\text{NO}}, \tag{9}$$

where Y_{NO} is the NO mass fraction, D is the effective diffusion coefficient, S_{NO} is the source term.

2.3 Boundary conditions

In this paper, no slip and adiabatic boundary were set up for all the walls of the combustor. The pressure outlet boundary was specified at the combustor outlet. Mass flow inlet boundary was set for the fuel and air inlet. The mass flow rate, temperature and pressure of air are 2,7 kg/s, 673 K and 1,01325 MPa respectively. There are four types of fuels sprayed from the dual-fuel nozzle into the combustor, and the parameters of the fuels are in Tab. 1.

Table 1 Fuel inlet variables

Conditions	Mass flow rate, kg/s			Temperature, K		
	Liquid fuel	Reformed gas	Steam	Liquid fuel	Reformed gas	Steam
Case 1	0,066670			300	723	723
Case 2	0,066670		0,013334	300	723	723
Case 3	0,033335	0,15235		300	723	723
Case 4		0,30470		300	723	723

The liquid fuel is $C_{12}H_{23}$ in this work. The steam in the Case 2 is sprayed into the combustor from the gas channel of the dual-fuel nozzle, and the steam mass flow rate is 20 % of the liquid fuel mass flow rate. The enthalpies of the fuels in Case 1, 3 and 4 are kept constant. However, the enthalpy of the fuel in Case 2 is higher than the other cases due to the additional enthalpy of steam. The volume fraction of reformed gas is CO～6,04 %, H_2～43,61 %, CO_2～10,74 %, H_2O～39,61 %.

2.4 Model validation

Numerical approach was validated by a dual swirling model combustor developed by Nanjing University of Aeronautics and Astronautics. Detailed structure of the model combustor can be referred to Ref. [19]. The boundary conditions of the experimental and numerical cases are as follows: air mass flow rate is 0,24 kg/s, the temperature is 500 K, the pressure is 0,13 MPa; oil mass flow rate is 0,00468 kg/s, the temperature is 300 K. The simulation and experimental data comparisons are shown in Fig. 3. From the comparison of both temperature and the CO_2 mass fraction radial profiles at combustor outlet, it is shown that the adopted numerical approach in this paper gives a reasonable prediction of combustor.

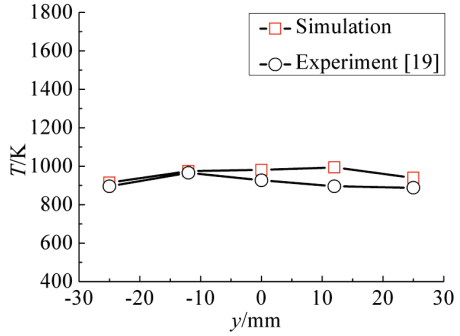

(a) Temperature

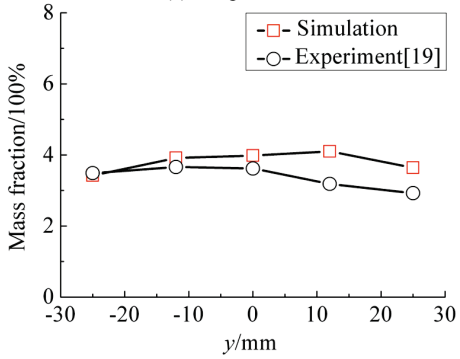

(b) CO_2 mass fraction

Figure 3 Temperature and CO_2 mass fraction radial profiles at combustor outlet

3 Result and discussion

The combustor performance was evaluated through the analysis of the temperature and species distribution for different fuels.

3.1 Temperature distribution

Fig. 4 shows the temperature distribution inside the CRGT combustor for the liquid fuel, liquid fuel + steam, liquid fuel + reformed gas and reformed gas respectively. As seen in Fig. 4, obvious differences are observed on the flame temperatures and structures respectively for the four cases. The maximum flame temperature inside the combustor is obtained for liquid fuel, which is 2258 K. The maximum flame temperature in Case 2 (liquid fuel + steam), Case 3 (liquid fuel + reformed gas) and Case 4 (reformed gas) are 2083, 2151 and 2026 K, respectively. As seen in Figs. 4 (a), (c) and (d), due to the high volume fraction of H_2O in reformed gas, the maximum flame temperature inside the combustor decreases as the percentage of reformed gas in the fuel increases. This would allow greater flexibility for controlling temperature and improving combustor performance. As it is shown in Fig. 4, due to the vaporization process of liquid fuel, a low temperature region in the central recirculation zone is obtained for the former three cases respectively. However, due to the rapidly mixing of reformed gas and air, the temperature in the central recirculation zone in Case 4 is higher than that in the former three cases.

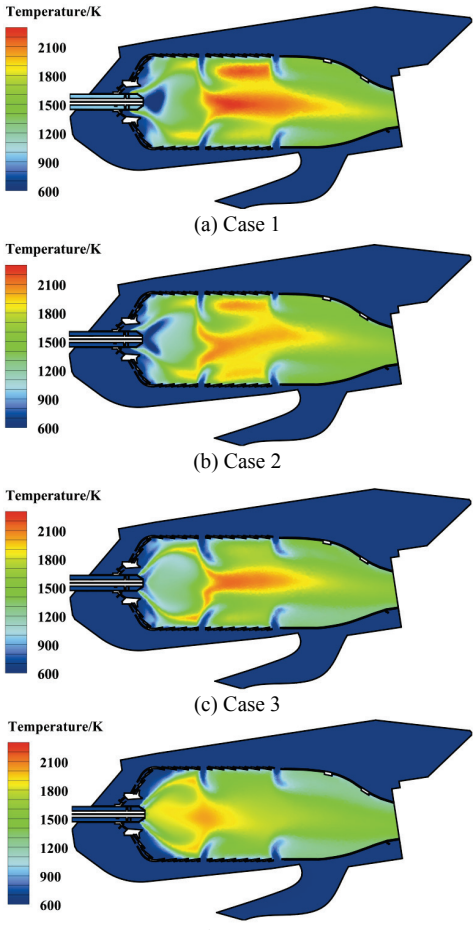

(a) Case 1

(b) Case 2

(c) Case 3

(d) Case 4

Figure 4 Temperature distributions in combustor meridian plane

In order to study the effect of the fuel on the temperature distribution in detail, the 1800 K isosurface in the combustor meridian plane is shown in Fig. 5. The temperature is larger than 1800 K inside the isosurface and it rapidly decays to lower values outside the isosurface (see Fig. 4). As seen in Figs. 5 (a) and (b), the length of high temperature region in Case 2 is shorter than that in Case 1. It is because the steam has taken in more heat to reach the equilibrium temperature. As already mentioned, the volume fraction of H_2O is high in the reformed gas and the reformed gas can mix and combust with air faster than liquid fuel. Thus, the high temperature region in combustor becomes smaller and closer to the nozzle as the percentage of reformed gas in the fuel increases (shown in Figs. 5 (a), (c) and (d)).

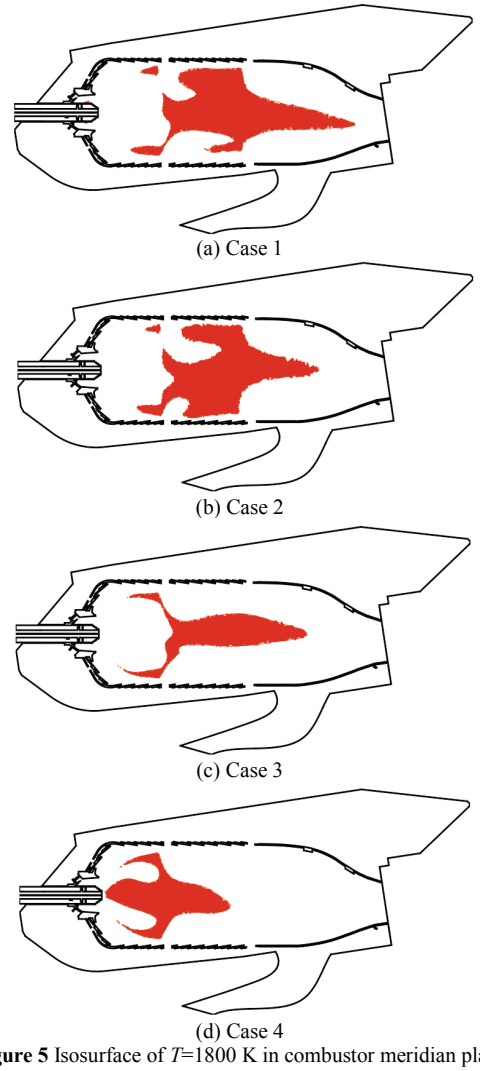

(a) Case 1

(b) Case 2

(c) Case 3

(d) Case 4

Figure 5 Isosurface of T=1800 K in combustor meridian plane

To help understand the temperature distribution, temperature profile along the central axis in flame tube is shown in Fig. 6. In each case, there is a peak temperature followed by a gradual decline down the length of the combustor. Due to more fuel consumed as the central axis increases, the temperature increases along the central axis. Furthermore, as the fuel becomes less and dilution air becomes more, the temperature decreases gradually along the central axis. As seen in Fig. 6, in the region from nozzle to x=0,17 m, due to the liquid droplets evaporation process, the temperatures in the former three cases are

lower than that in Case 4. It can also be seen from the figure that the maximum temperature can be obtained when the liquid fuel is adopted in the combustor. The maximum temperatures for the four cases are 2245, 2030, 2150 and 2016 K, respectively. It illustrates that both injecting the steam into the combustor and replacing the liquid fuel by reformed gas in the combustor can lower the temperature effectively.

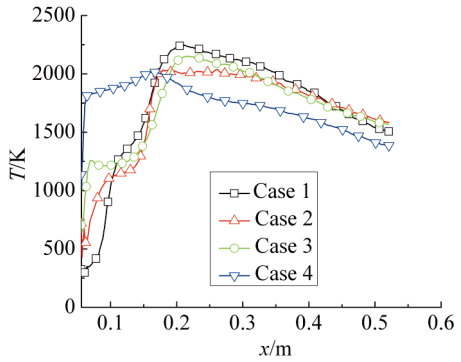

Figure 6 Temperature profile along central axis in flame tube

The average temperature of combustor wall is shown in Fig. 7. As seen in Fig. 7, due to the higher combustion temperature in the combustor for Case 1, the average temperature of combustor wall for Case 1 is higher than those for the other three cases. The average temperatures of combustor wall for the four cases are 1085, 1033, 1037 and 1024 K, respectively. It illustrates that both injecting the steam into the combustor and replacing the liquid fuel by reformed gas in the combustor can lower the combustor wall temperature, which is useful to prolong the service life of combustor liner.

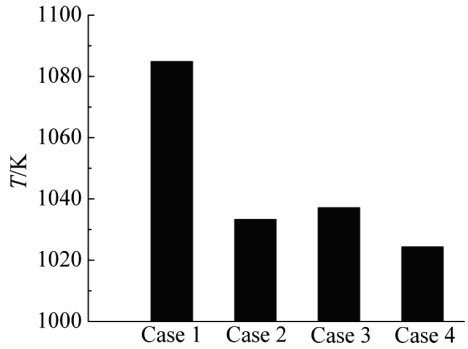

Figure 7 Average temperature of combustor wall

Fig. 8 shows the temperature distribution on combustor outlet for the four cases. As seen in Figs. 8 (a) and (b), the maximum temperature of combustor outlet changes little, however the location of high temperature region is closer to the left side of the outlet. As seen in Figs. 8 (a) and (c) and (d), the outlet temperature decreases as the percentage of reformed gas in the fuel increases. Since the rotational direction of the reformed gas is opposite to that of the air from swirler, the temperature distribution on the combustor outlet for Case 3 and 4 is more symmetrical than that for Case 1.

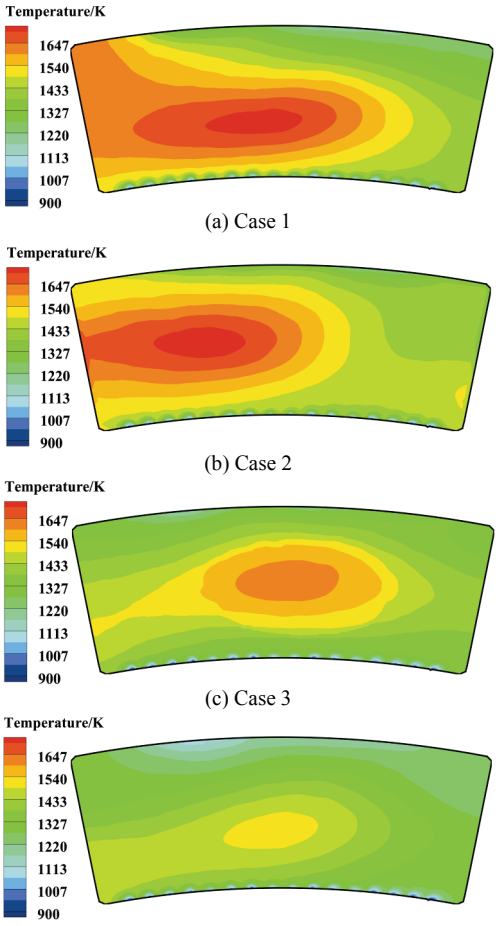

(a) Case 1

(b) Case 2

(c) Case 3

(d) Case 4

Figure 8 Temperature distributions on combustor outlet

The temperature distribution factor of combustor outlet has a strong impact on the gas turbine blade. Fig. 9 shows the Temperature distribution factor of combustor outlet. The overall temperature distribution factor (*OTDF*) and radial temperature distribution factor (*RTDF*) are defined respectively as follows:

$$OTDF = \frac{T_{t4\max} - T_{t4}}{T_{t4} - T_{t3}}, \tag{10}$$

$$RTDF = \frac{T_{t4r\max} - T_{t4}}{T_{t4} - T_{t3}}, \tag{11}$$

where $T_{t4\max}$ is combustor outlet maximum temperature, $T_{t4r\ \max}$ is combustor outlet radial maximum temperature, T_{t4} is combustor outlet average temperature, T_{t3} is air inlet temperature.

As seen in Fig. 9 (a), compared with Case 1, the *OTDF* is a little bigger when the steam is injected into the combustor. However, the *OTDF* decreases as the percentage of reformed gas in the fuel increases. As seen in Fig. 9 (b), the *RTDF* in Case 2 is the lowest and in Case 1 is the highest. In summary, the combustor outlet temperature distribution can be improved when the reformed gas is adopted in combustor, in comparison with the liquid fuel. Compared with the liquid fuel combustor, injecting steam into combustor will improve the radial temperature distribution of combustor outlet, but a little deterioration for the overall temperature distribution.

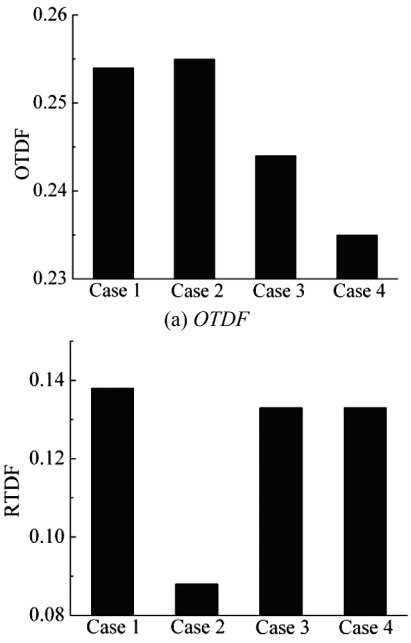

(a) *OTDF*

(b) *RTDF*

Figure 9 Temperature distribution factor

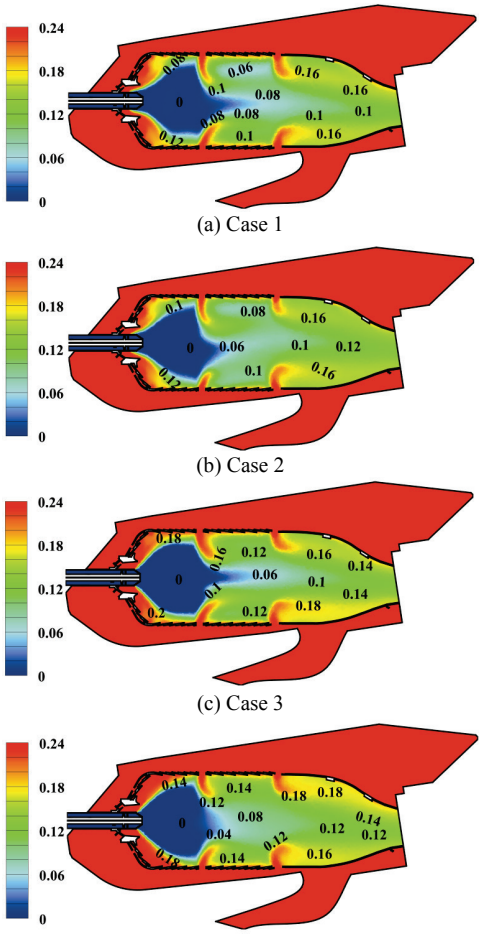

(a) Case 1

(b) Case 2

(c) Case 3

(d) Case 4

Figure 10 O_2 mass fraction distributions

3.2 Species distribution

Fig. 10 shows the mass fraction of O_2 distribution in the combustor meridian plane. The analysis of O_2 mass fraction distribution indicates how the fuel is consumed inside the combustor. As can be seen from the figure, due to the combustion process, there is little O_2 in the central recirculation zone of the combustor for the four cases. Furthermore, lower O_2 values in other region of the combustor are observed which illustrates the fuels are still being consumed. At the combustor outlet, the O_2 concentration is approximately uniform for the four cases.

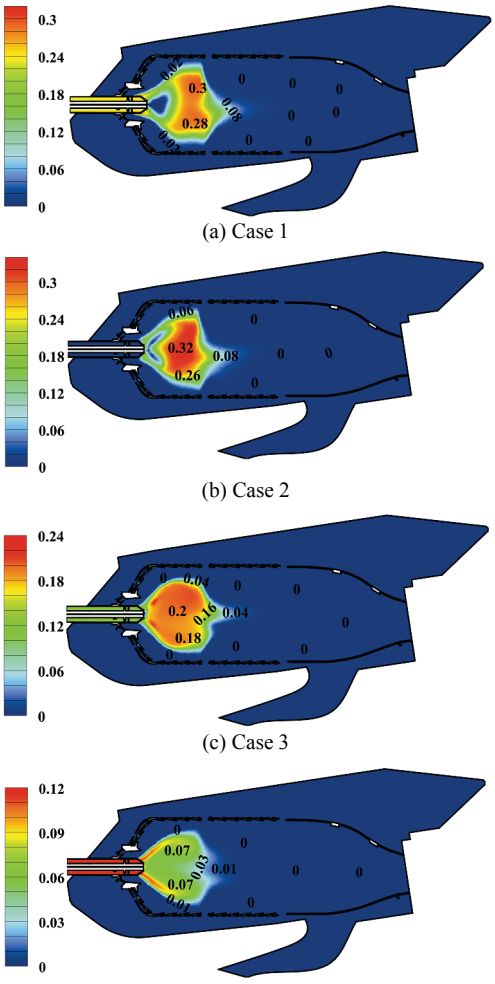

(a) Case 1

(b) Case 2

(c) Case 3

(d) Case 4

Figure 11 CO mass fraction distribution

Fig. 11 presents the CO mass fraction distribution in the combustor meridian plane. The CO mass fraction distribution can reflect the complete level of fuel combustion. As seen in Fig.11, the fuel can be combusted completely in the combustor for the four cases. As seen in Fig. 11, the maximum value of CO mass fraction is higher for Case 2 than Case 1. It illustrates that the consumption rate of the fuel ($C_{12}H_{23}$) can be reduced by steam in the primary combustion zone of combustor. It is also noted that due to the low CO fraction in the reformed gas, the maximum value of CO mass fraction decreases as the percentage of reformed gas in the fuel increases (see Figs. 11(a), (c) and (d)).

3.3 NO emission

The NO mass fraction distribution inside the combustor for the liquid fuel, liquid fuel + steam, liquid fuel + reformed gas and reformed gas is shown in Fig. 12. As seen in Fig. 12, the NO mass fraction distribution is

similar to the temperature distribution inside the combustor. The maximum NO mass fraction is obtained for the liquid fuel. As seen from Figs. 12 (a) and (b), compared with the liquid fuel, NO mass fraction is lower in Case 2 (liquid fuel + steam) as the flame temperature decreases. As already mentioned, the plenty of H_2O in the reformed gas has resulted in the flame temperature inside combustor decreasing as percentage of reformed gas in the fuel increases. Thus, the NO mass fraction in the combustor decreases as the percentage of reformed gas in the fuel increases (see Figs.12 (a), (c) and (d)).

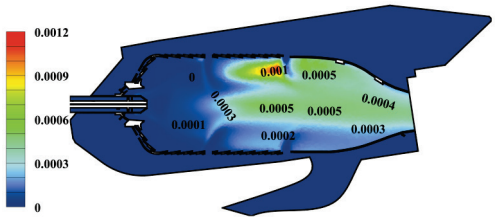

(a) Case 1

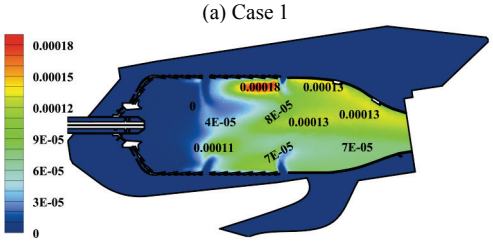

(b) Case 2

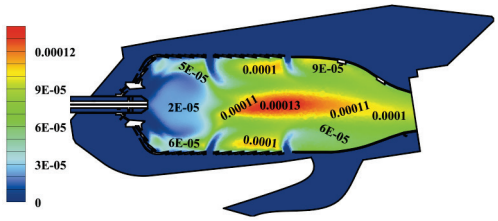

(c) Case 3

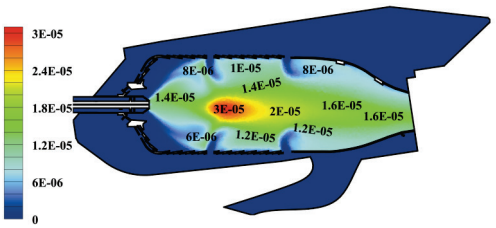

(d) Case 4

Figure 12 NO mass fraction distribution

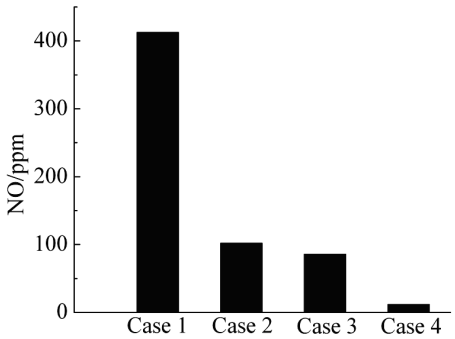

Figure 13 NO emission at combustor outlet

Fig. 13 presents the comparison of the NO emission at combustor outlet for the liquid fuel, liquid fuel + steam, liquid fuel + reformed gas and reformed gas. As can be seen in Fig. 13, the maximum value of NO emission is obtained for liquid fuel and the minimum value is obtained for reformed gas. The NO emission for the liquid fuel, liquid fuel + steam, liquid fuel + reformed gas and reformed gas are 413, 102, 86 and 12 ppm, respectively. It illustrates that injecting the steam into the combustor and replacing the liquid fuel by reformed gas in the combustor are both effective methods to reduce the NO emission in the combustor, in comparison with liquid fuel combustor. And the effect of the latter method is better.

4 Conclusions

Numerical simulation was carried out in this study to investigate the combustion performance and emissions for the CRGT combustor. There are four combustion processes in the combustor: liquid fuel, liquid fuel + steam, liquid fuel + reformed gas and reformed gas. The PDF model, realizable model and SIMLPLE algorithm were used to solve the governing equations. The flame temperature and species concentration distributions inside the combustor were obtained.

The results show that the four combustion process can be achieved in a dual-fuel combustor for CRGT. And the fuels for the four cases can burn effectively in the combustor. For the liquid fuel combustor, the NO emission is 413 ppm which does not meet the requirements.

Compared with the liquid fuel combustor, the flame temperature, average temperature of combustor wall and NO emission are reduced by 7,8 %, 4,8 % and 75,3 %, respectively when the steam is injected into the combustor. The radial temperature distribution of combustor outlet is improved when the steam is injected into the combustor, but the overall temperature distribution of combustor outlet deteriorates a little.

The flame temperature, average temperature of combustor wall and NO emission at combustor outlet decrease as the percentage of the reformed gas in fuel increases. When the combustor is fuelled with reformed gas, the flame temperature, average temperature of combustor wall and NO emission are reduced by 10,3 %, 5,6 % and 97,2 %, respectively, in comparison with the liquid fuel combustor. And the temperature distribution of the combustor outlet can be improved when the liquid fuel is replaced by the reformed gas.

Based on the analysis of the combustion process in the CRGT combustor, it may be concluded that both injecting steam into the combustor and replacing the liquid fuel by reformed gas can provide longer life for the combustor liner, as well as less amount of pollutants, in comparison with the liquid fuel combustor. On the other hand, the latter method can lower the NO emission more effectively and with a better temperature distribution of combustor outlet.

5 References

[1] Nieckele, A. O.; Naccache, M. F.; Gomes, M. S. P. Combustion performance of an aluminum melting furnace operating with natural gas and liquid fuel. // Applied Thermal Engineering. 31, (2011), pp. 841-851.

[2] Nakagaki, T.; Ogawa, T.; Hirata, H.; Kawamoto, K.; Ohashi, Y.; Tanaka, K. Development of Chemically Recuperated Micro Gas Turbine. // Journal of Engineering

for Gas Turbines and Power. 125, 1(2003), pp. 391-397.
[3] Sharma, N. Y.; Som, S. K. Influence of fuel volatility and spray parameters on combustion characteristics and NOx emission in a gas turbine combustor. // Applied Thermal Engineering. 24, 5-6(2004), pp. 885-903.
[4] Li, L.; Peng, X. F.; Liu, T. Combustion and cooling performance in an aero-engine annular combustor. // Applied Thermal Engineering. 26, (2006), pp. 1771-1779.
[5] Benini, E.; Pandolfo, S.; Zoppellari, S. Reduction of NO emissions in a turbojet combustor by direct water/steam injection: Numerical and experimental assessment. // Applied Thermal Engineering. 29, 17-18(2009), pp. 3506-3510.
[6] Furuhata, T.; Kawata, T.; Mizukoshi, N.; Arai, M. Effect of steam addition pathways on NO reduction characteristics in a can-type spray combustor. // Fuel. 89, 10(2010), pp. 3119-3126.
[7] Koyama, M.; Fujiwara, H. Development of a dual-fuel gas turbine engine of liquid and low-calorific gas. // JSME International Journal Series B. 49, 2(2006), pp. 224-229.
[8] Gobbato, P.; Masi, M.; Toffolo, A.; Lazzaretto, A. Numerical simulation of a hydrogen fuelled gas turbine combustor. // International Journal of Hydrogen Energy. 36, 13(2011), pp. 7993-8002.
[9] Seibert, M.; Nieh, S. Simulation of dual firing of hydrogen-rich reformate and JP-8 surrogate in a swirling combustor. // International Journal of Hydrogen Energy. 38, 14(2013), pp. 5911-5917.
[10] Ghenai, C. Combustion of Syngas Fuel in Gas Turbine Can Combustor. // Advances in Mechanical Engineering. 2010, (2010), pp. 1-13.
[11] Wang, H.; Luo, K.; Lu, S. Q.; Fan, J. R. Direct numerical simulation and analysis of a hydrogen/air swirling premixed flame in a micro combustor. // International Journal of Hydrogen Energy. 36, 21(2011), pp. 13838-13849.
[12] Tanaka, S.; Shimura, M.; Fukushima, N.; Tanahashi, M.; Miyauchi, T. DNS of turbulent swirling premixed flame in a micro gas turbine combustor. // Proceedings of the Combustion Institute. 33, 2(2011), pp. 3293-3300.
[13] Arghode, V. K.; Gupta, A. K. Hydrogen addition effects on methane-air colorless distributed combustion flames. // International Journal of Hydrogen Energy. 36, 10(2011), pp. 6292-6302.
[14] Kumar, P. K. E.; Mishra, D. P. Numerical simulation of cavity flow structure in an axisymmetric trapped vortex combustor. // Aerospace Science and Technology. 21, 1(2012), pp. 16-23.
[15] Cameretti, M. C.; Tuccillo, R.; Piazzesi, R. Study of an exhaust gas recirculation equipped micro gas turbine supplied with bio-fuels. // Applied Thermal Engineering. 59, 1-2(2013), pp. 162-173.
[16] ANSYS, Inc, ANSYS Fluent 12.0 Theory Guide, January 2009.
[17] Shih, T. H.; Liou, W. W.; Shabbir, A.; Yang, Z.; Zhu, J. A new eddy-viscosity model for high Reynolds numerical turbulent flows-model development and validation. // Computers Fluids. 24, 3(1995), pp. 227-238.
[18] Hashemi, S. A.; Fattahi, A.; Sheikhzadeh, G. A.; Mehrabian, M. A. Investigation of the effect of air turbulence intensity on NOx emission in non-premixed hydrogen and hydrogen-hydrocarbon composite fuel combustion. // International Journal of Hydrogen Energy. 36, 16(2011), pp. 10159-10168.
[19] Dang, X. X. Experimental investigation and numerical simulation of a gas turbine annular combustor with dual-stage swirler. // Ph.D. Thesis, Nanjing University of Aeronautics and Astronautics, 2009.

Authors' addresses

Gang Pan, Hongtao Zheng
College of Power and Energy Engineering,
Harbin Engineering University,
Harbin 150001, China
E-mail: markpg0808@gmail.com